

HIGH-EFFICIENCY AMORPHOUS SILICON ALLOY BASED SOLAR CELLS AND MODULES

**Quarterly Technical Progress Report
December 1, 2004 through February 28, 2005**

**S. Guha and J. Yang
United Solar Ovonic Corporation
Troy, Michigan**

NREL Technical Monitor: Bolko von Roedern

Prepared under Subcontract No. ZDJ-2-30630-19

TABLE OF CONTENT

Overview	2
1. Optimization of Ag/ZnO back reflector	3
1.1 INTRODUCTION	3
1.2 EXPERIMENTAL	3
1.3 RESULTS AND DISCUSSION	3
1.3.1. Texture and light scattering of Ag/ZnO back reflector.....	4
1.3.2. a-SiGe:H bottom cells on various BR substrates.....	7
1.3.3. nc-Si:H solar cells on various BR substrates	10
1.4 SUMMARY	11
2. nc-Si:H single junction solar cells made by MVHF method at high deposition rates	12
2.1. INTRODUCTION	12
2.2. nc-Si:H SINGLE-JUNCTION AND a-Si:H/nc-Si:H DOUBLE-JUNCTION SOLAR CELLS	12
2.3 SUMMARY	14
3. Large-area deposition of nc-Si:H solar cells at high deposition rate	17
4. References.....	19

Overview

This report covers the work from December 1, 2004 to February 28, 2005 at United Solar Ovonic Corporation under the thin film partnership program supported by NREL. In this quarter, we have worked in the following areas:

1. We have continued to work on the optimization of Ag/ZnO back reflector (BR) for a-SiGe:H and nc-Si:H solar cells. In the last quarter, we have improved the deposition process for the Ag and ZnO layers by changing the deposition process to modify the surface morphology to achieve a high light trapping effect. In this quarter, we used chemical etching to modify the BR subsurface. We systematically studied the correlation of the fabrication process of BR, surface morphology measured by AFM, and solar cell performance. The experimental results show that the BRs with large micro-features increase the short-circuit current density (J_{sc}) of nc-Si:H by enhancing long wavelength response and improve the open-circuit voltage (V_{oc}) of a-SiGe:H bottom cells by reducing back diffusion and shunt current density.
2. In the area of high rate deposition, we have continued to work on nc-Si:H using MVHF glow discharge. We have explored a new deposition regime under high pressure to enhance the deposition rate. Currently, we are working at $\sim 6\text{-}10 \text{ \AA/s}$ corresponding to an intrinsic layer deposition time of 20-30 minutes. We have achieved an initial active-area efficiency of 8.2% for a nc-Si:H single-junction solar cell, where the intrinsic layer was deposited for 30 minutes.
3. In the task on large-area deposition, we have focused on the nc-Si:H solar cells at high deposition rates. Currently, the deposition rate is around $3\text{-}5 \text{ \AA/s}$, corresponding to an intrinsic layer deposition time of 50-60 minutes. We have achieved an initial active-area (0.25 cm^2) efficiency of 12% using an a-Si:H/nc-Si:H double-junction structure. Currently, we are using the new recipe to make large-area modules. In addition, we have light-soaked the mini-modules (aperture area of 45 cm^2) made in the last quarter. Those modules showed an initial aperture-area efficiency of 11.3% and stabilized to 10.2%.

1. Optimization of Ag/ZnO back reflector

1.1 INTRODUCTION

Hydrogenated amorphous silicon (a-Si:H) and silicon germanium (a-SiGe:H) alloy based solar cell technology is one of the most attractive photovoltaic technologies, due to its low cost and large-scale manufacturing abilities. Among the techniques for improving cell performance, light trapping with textured back reflector (BR) is an important one for enhancing short-circuit current density, J_{sc} [1]. A textured Ag/ZnO BR was used for achieving 14.6% initial and 13.0% stable cell efficiencies in an a-Si:H/a-SiGe:H/a-SiGe:H triple-junction structure [2]. Recently, hydrogenated nanocrystalline silicon (nc-Si:H) solar cell has attracted remarkable attention due to its superior long wavelength response and improved stability over a-SiGe:H [3]. Using our conventional Ag/ZnO BR, we have achieved high efficiencies with a-Si:H/nc-Si:H double-junction and a-Si:H/a-SiGe:H/nc-Si:H triple-junction structures [4,5]. However, because of the nature of the nc-Si:H structure, the optimized Ag/ZnO BR used for the a-Si:H and a-SiGe:H solar cells may not necessarily be the best choice for the nc-Si:H solar cells. Optimizing the Ag/ZnO BR has the potential of improving the nc-Si:H cell efficiency further, hence achieving even higher efficiencies in multi-junction cells with nc-Si:H bottom cell. In addition, an improved BR may result in an even higher efficiency for a-Si:H/a-SiGe:H/a-SiGe:H triple-junction cells. In the last quarter, we worked on the optimization of the Ag/ZnO BR by searching the deposition parameter space and also made some improvement in a-SiGe:H and nc-Si:H solar cell performance. In this quarter, we have continued this work. At the same time, we have used HCl etching to modify the surface morphology of various BRs. We report the results on the correlation of BR preparation condition, surface morphology on BRs and solar cell performance.

1.2 EXPERIMENTAL

We deposited Ag/ZnO BR on specular stainless steel substrates using a sputtering method. The texture of the Ag and ZnO layers was controlled by deposition parameters such as pressure, substrate temperature, and RF power. In addition, we used chemical etching with 0.5% HCl [6] to modify the texture on the BR surface. The surface morphology was investigated by atomic force microscopy (AFM) at NREL. To characterize the scattering effect from the textured surface, the scattered light intensity from a He-Ne laser, which illuminates the sample perpendicularly to the sample surface, was measured at different angles. Details of the measurements are given in the last quarterly report. Finally, a-SiGe:H and nc-Si:H solar cells were deposited on BR substrates made under various conditions to correlate the surface properties of the BR to the solar cell performance. The solar cells were deposited using RF glow discharge at low rates in different deposition systems. Current density versus voltage, J-V, characteristics were measured under an AM1.5 solar simulator at 25 °C. Quantum efficiency, QE, was measured from 300 to 1000 nm at room temperature.

1.3 RESULTS AND DISCUSSION

1.3.1. Texture and light scattering of Ag/ZnO back reflector

The texture of the Ag/ZnO BR can be controlled by the sputtering parameters such as substrate temperature, gas flow rate, RF power, and the thickness of the Ag and ZnO layers. A proper chemical etching can also modify the surface morphology. Figure 1 shows four AFM pictures of BRs made under various conditions and chemical treatments, where (a) is a conventional BR (5BR1748) developed previously [1], (b) a BR (R7900) with large micro-features created by adjusting the deposition parameter, (c) is a BR (R7948) with a thicker ZnO before chemical etching, and (d) the same BR as in (c), but after 30-second chemical etching in 0.5% HCl. The micro-feature size on the conventional BR is on the order of 0.1-0.2 μm with a root mean square (RMS) roughness of 38.2 nm. By adjusting the deposition parameters, we can increase the feature size to as large as 0.5-1.0 μm with RMS of 80.5 nm (Fig. 1 (b)). In addition, the chemical etching modifies the micro-features on the BR surface. It seems that the small features are etched away and the feature size increases. Correspondingly, the RMS increases from 39.6 nm to 63.2 nm after 30-second etching in 0.5% HCl as shown by comparing Fig. 1 (c) and (d).

Figure 2 (a) plots the RMS versus the etching time for three BRs with different initial RMS. It clearly shows that RMS increases after etching. The four samples with lower initial RMS, the RMS increase with the etching time up to 20 seconds. No additional roughness increase was observed for etching time longer than 20 seconds. For one sample (R7900) with an initial RMS of 80 nm, the RMS increases to 140 nm after 30-second etching. Figure 2 (b) shows the difference between the total microscopic surface area and the flat surface area. It does not show a unique trend of the area difference. If we assume that the surface micro-features are all pyramids, the angles between the feature surface and base are in the range of 27 and 38°.

The upper plot in Fig. 3 shows the measured scattered light intensity, $I(\theta)$, versus the angle, θ , between the scattering beam and the sample surface, where the laser is incident from 90°. The lower plot shows the total scattered light intensity, $I(\theta)\cos\theta$, at all the positions with

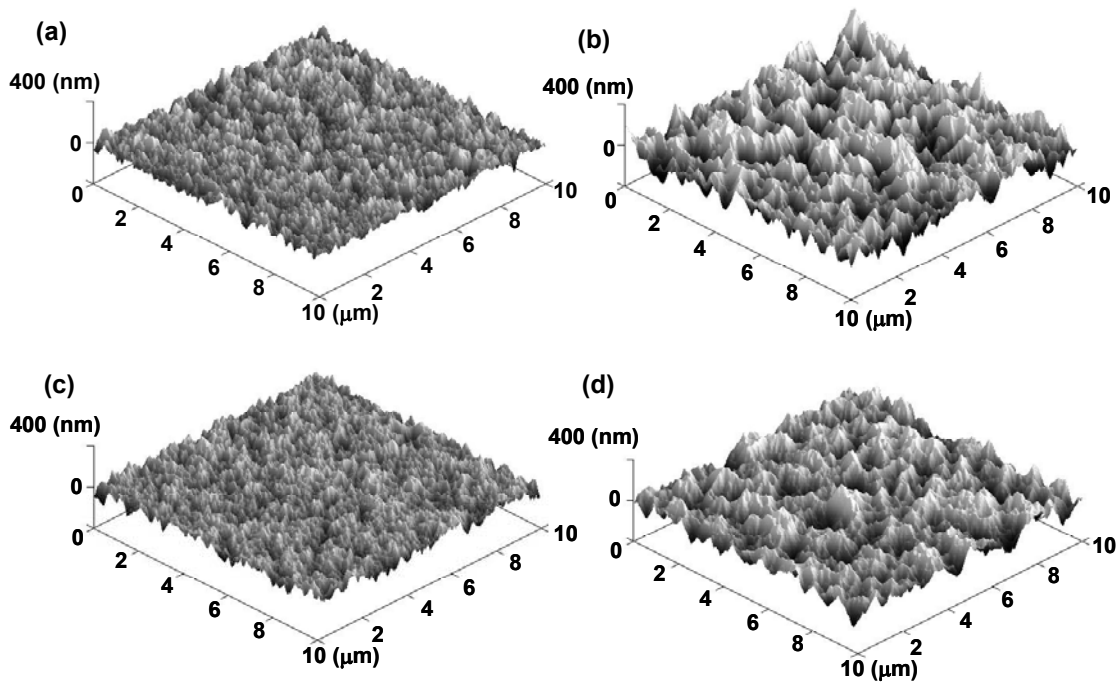


Figure 1. AFM pictures of four Ag/ZnO BRs made with various deposition parameters and chemical etchings. Details of the sample preparation are given in the text.

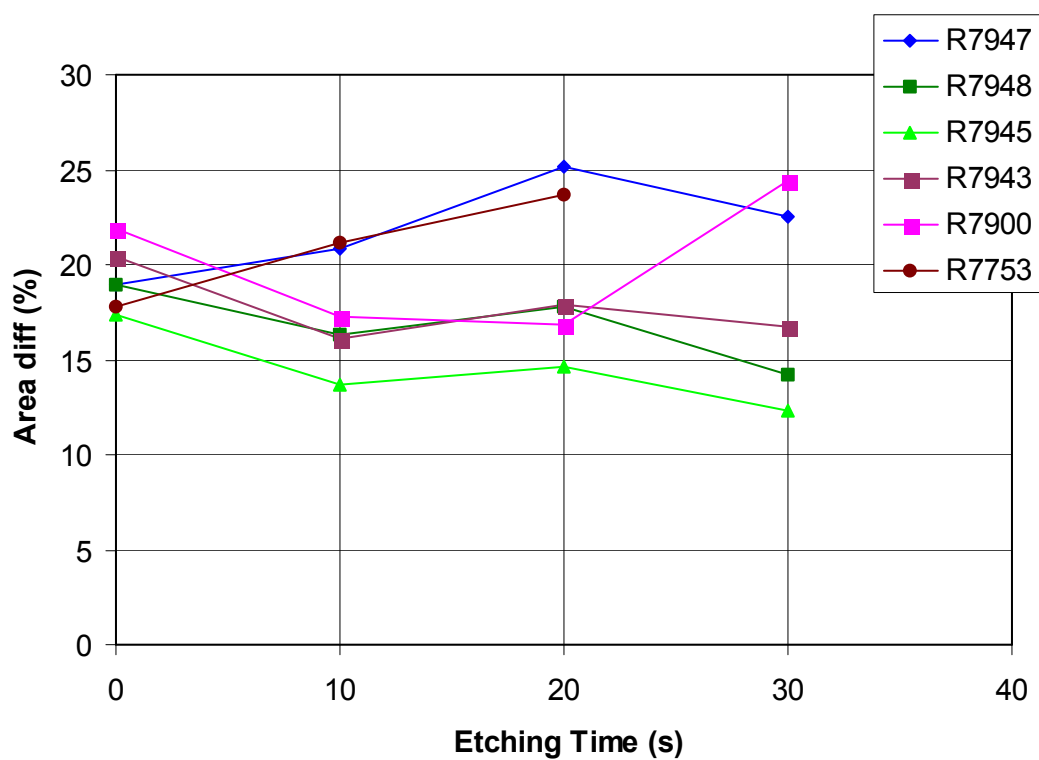
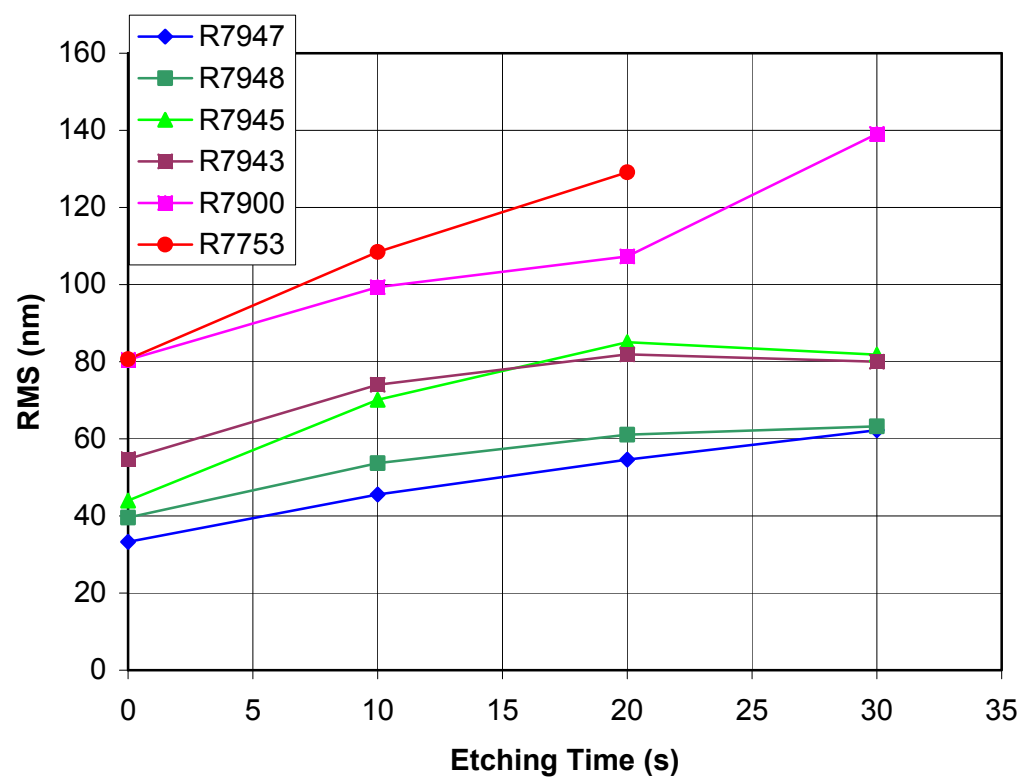


Figure 2. (upper) RMS and (lower) area-difference versus the etching time in 0.5% HCl for Ag/ZnO BRs with different original roughness.

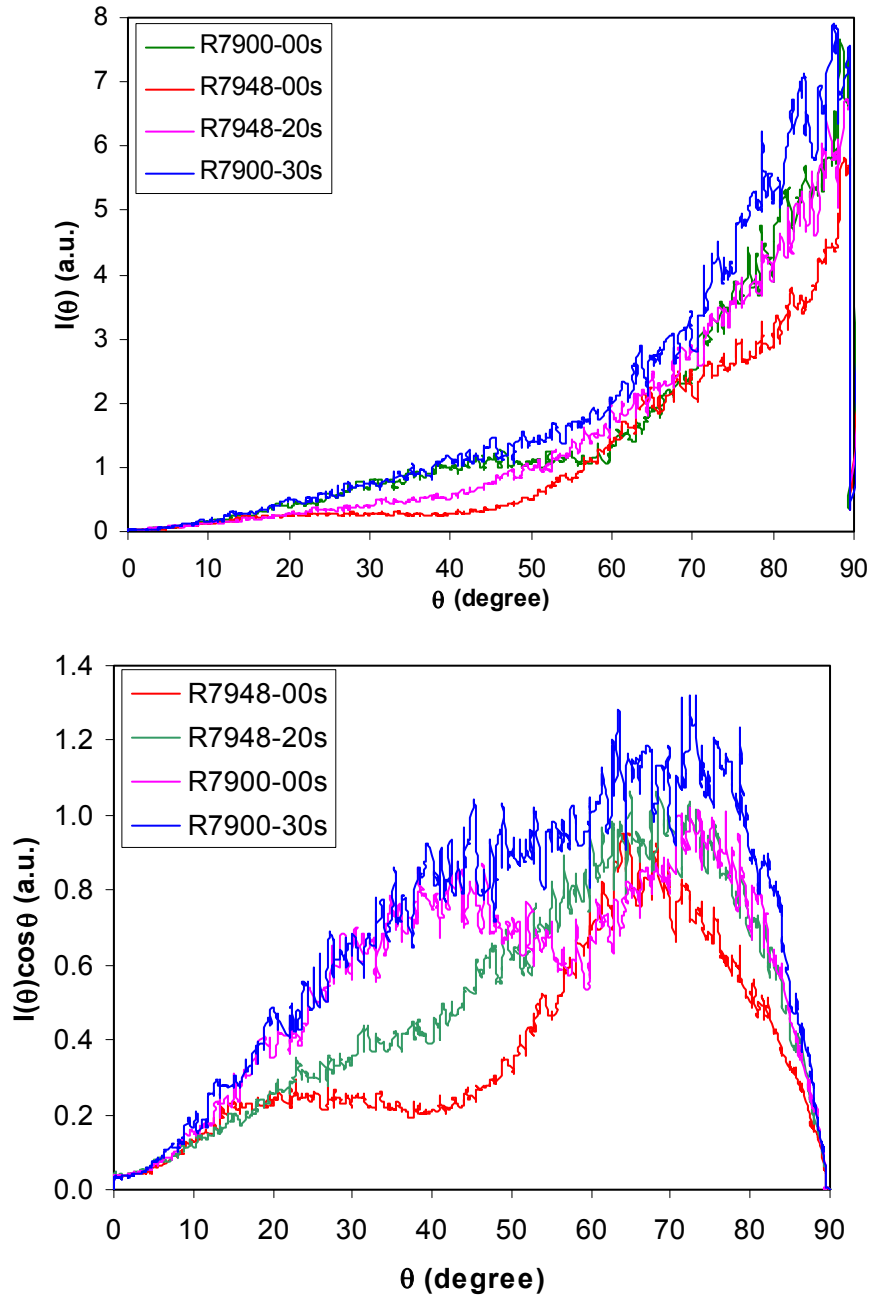


Figure 3. (a) Scattered light intensity, $I(\theta)$, versus the angle, θ , between the detector and the sample surface, (b) the $I(\theta)\cos\theta$ versus θ .

the same θ , where $\cos\theta$ takes into account the geometry factor. In the figure, sample R7948 has an initial RMS of 39.2 nm and the RMS increases to 63.2 nm after 30-second etching; while sample R7900 has an initial RMS of 80.5 nm and 139.2 nm after-30 second etching. Since the angle between the micro-feature surface and the base does not change very much, the increase of RMS is mainly due to the increase of the feature size. Because the light cannot distinguish the features with sizes much smaller than the wavelength of the light, the BRs with small micro-features do not scatter the light effectively. With the increase of the micro-feature size, the scattered light intensity increases. Another interesting phenomenon is the fine structures on the scattered light curves as shown in Fig. 3. We initially thought they were measurement noise, but later on we found they are real signals and can be reproduced by repeated measurement without changing the position of the sample. Further investigation of possible correlation between the micro-features on the BR surface and scattered light intensity is under way.

1.3.2. a-SiGe:H bottom cells on various BR substrates

The final qualification for BR is to check whether it improves the solar cell performance. We deposited a-SiGe:H alloy solar cells on the different BRs described above. The deposition conditions are given previously [2]. Table I lists the BR properties and corresponding a-SiGe:H solar cell performance, where the solar cells were made with a bottom cell recipe for a-Si:H/a-SiGe:H/a-SiGe:H triple-junction solar cells. The J-V characteristics were measured under an AM1.5 solar simulator with a 630-nm cut-on filter, and the J_{sc} was obtained from QE measurements. We find that, the overall solar cell performance is improved by increasing the micro-feature size. Although there is a large run-to-run variation, the J_{sc} shows a tendency to increase with the RMS as plotted in Fig. 4 (upper). However, the gain in J_{sc} is not as large as expected. Two possible mechanisms could explain the lack of strong correlation between the J_{sc} and the roughness of the substrate. First, for the substrate with micro-feature size smaller than the wavelength of the light, the light cannot distinguish the micro-features, and therefore, the small features do not contribute to the light trapping effectively. For example, for a wavelength

Table I: BR properties and a-SiGe:H alloy solar cell performance. The J-V characteristics were measured under an AM1.5 solar simulator with a 630-nm long pass filter; J_{sc} was obtained from QE.

Sample #	BR #	Etching (sec)	RMS (nm)	P_{max} (mW/cm ²)	J_{sc} (mA/cm ²)	V_{oc} (V)	FF
B8564	5BR1748	0	38.2	4.07	10.16	0.641	0.625
R8539	R7749	0	65.3	4.57	11.03	0.650	0.638
R8534	R7900	0	80.5	4.38	10.06	0.654	0.665
R8538	R7753	0	80.7	4.47	11.10	0.651	0.612
R8549	R7753	10	108.5	4.58	10.83	0.655	0.646
B8563	R7948	0	39.6	3.65	9.71	0.627	0.608
B8556	R7948	20	61.1	4.34	10.75	0.637	0.633
B8554	R7948	30	63.2	4.01	10.49	0.623	0.614
B8535	R7943	0	54.8	4.20	10.49	0.635	0.631
B8553	R7943	10	74.0	4.56	10.99	0.651	0.638
B8552	R7943	30	80.0	4.25	10.21	0.651	0.640

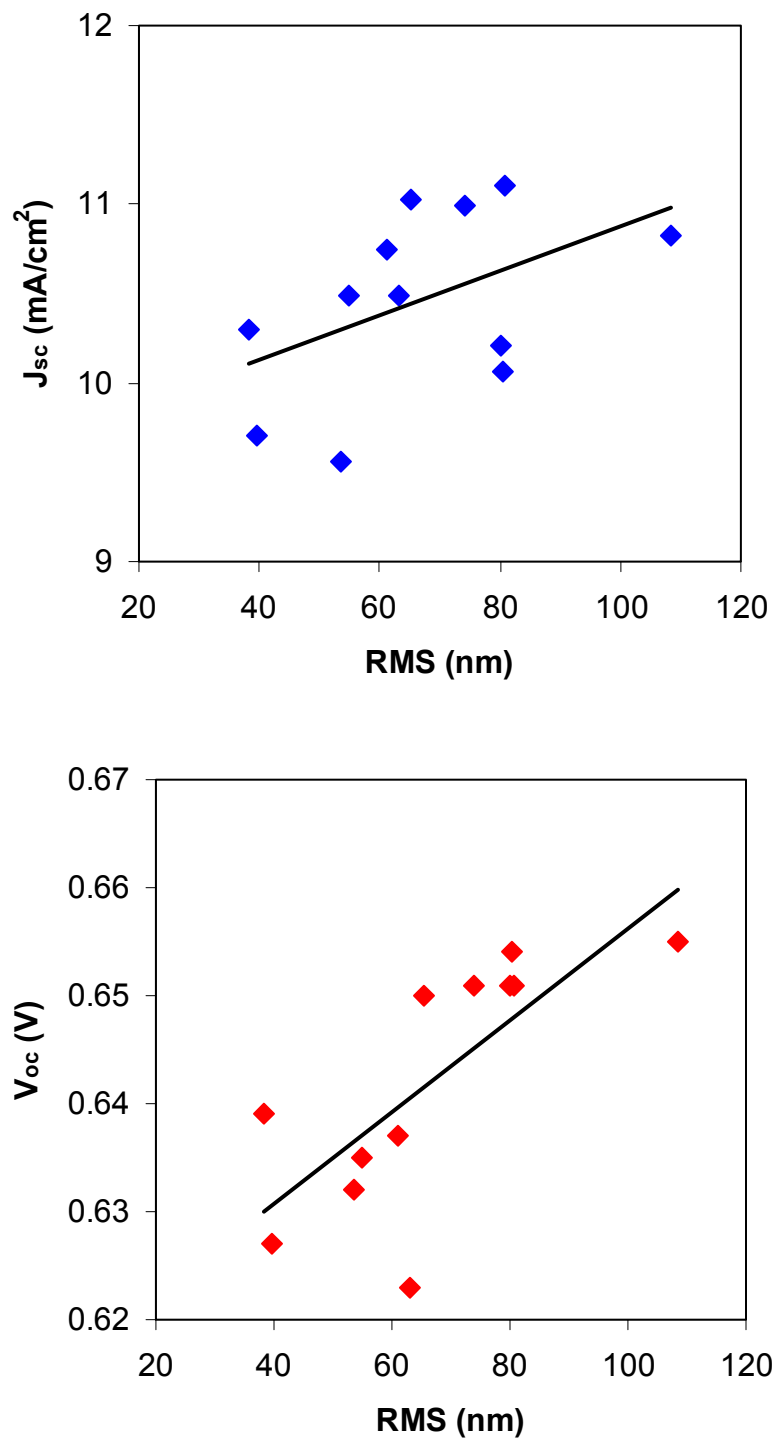


Figure 4. J_{sc} (upper) and V_{oc} (lower) versus the RMS of the Ag/ZnO BR substrates.

of 900 nm, by taking the wavelength compression factor of 3-4 ($n_{\text{Si}}/n_{\text{air}}$) into account, the micro-features with sizes smaller than 225-300 nm would not scatter the light effectively. The clear interference fringes on the QE curves for the cells on the BRs with smaller features as shown in Fig. 5 confirms the explanation. Second, for the BR with larger micro-features, the feature sizes could be larger than the cell thickness. Normally, for an a-SiGe:H bottom cell, the total thickness of the semiconductor layers is thinner than the long wavelength of the solar spectrum. If the semiconductor layers grow conformally with the substrate morphology, even though the micro-features can effectively scatter the light (as confirmed by the less interference on QE curves in Fig. 5), the light hardly reaches total reflection condition in the semiconductor layers. Therefore, the effect of texture on J_{sc} is not very large.

It is interesting to note that the open-circuit voltage, V_{oc} , increases for the cells deposited on the BR with a high RMS as shown by Fig. 4 (lower). This result was unexpected, but was confirmed by repeated experiments. One explanation could be that for the cells deposited on the BRs with smaller micro-features, the high density of sharp peaks on the substrate causes significant back diffusion of photo-generated carriers at the p/i and i/n interfaces. Sharp peaks can also cause an increase in the shunt current density. Increasing the micro-feature size is equivalent to decreasing the peak density, hence reducing the loss of V_{oc} .

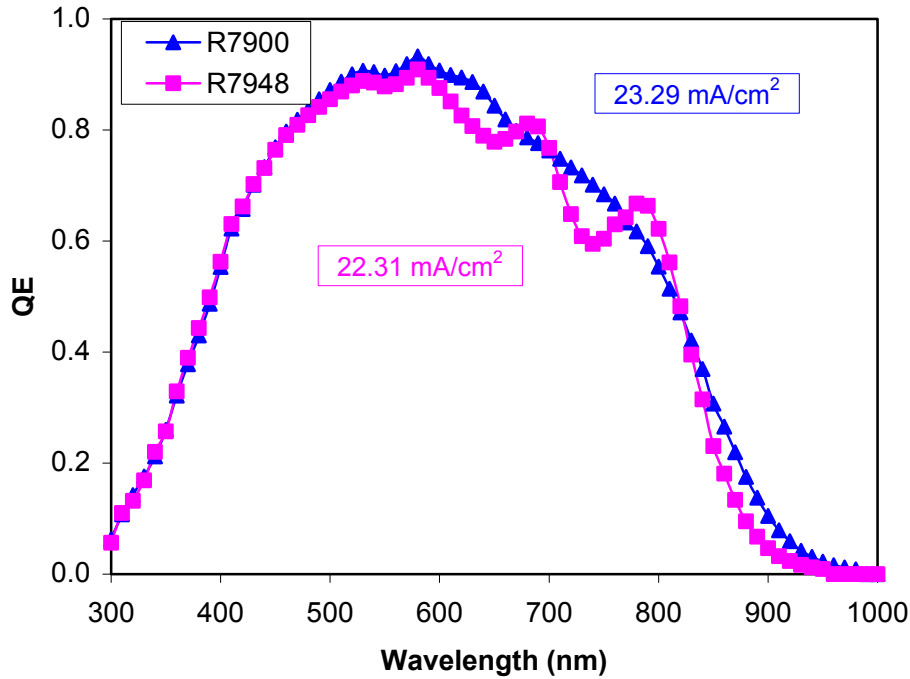


Figure 5. QE curves for a-SiGe:H bottom solar cells on R7900 and R7948 without etching.

Table II: BR properties and nc-Si:H solar cell performance. The J-V characteristics were measured under an AM1.5 solar simulator with J_{sc} obtained from QE.

Sample #	BR #	Etching (sec)	RMS (nm)	P_{max} (mW/cm ²)	J_{sc} (mA/cm ²)	V_{oc} (V)	FF
L15204	R7947	0	33.3	5.87	20.52	0.485	0.590
L15203	R7947	30	62.2	7.32	21.48	0.500	0.682
L15201	R7900	0	80.5	7.06	22.62	0.480	0.650
L15196	R7900	20	107.3	7.10	24.10	0.483	0.610

1.3.3. nc-Si:H solar cells on various BR substrates

We also deposited nc-Si:H cells on different BRs. Table II summarizes J-V characteristics along with the properties of the substrates, where the four solar cells were deposited under the same conditions. It clearly shows that the J_{sc} increases with the increase of the micro-feature size on the BR. Figure 6 plots the QE curves of the four nc-Si:H solar cells. Similar to the a-SiGe:H solar cell, the increase of micro-feature size eliminates the interference fringes from the QE curves, indicating a diffusive scattering in the device. The difference as compared to the a-SiGe:H cells is a clear gain in the J_{sc} obtained by increasing the roughness on the BR surface. The interpretation for the difference in the two cases could be as follows: the

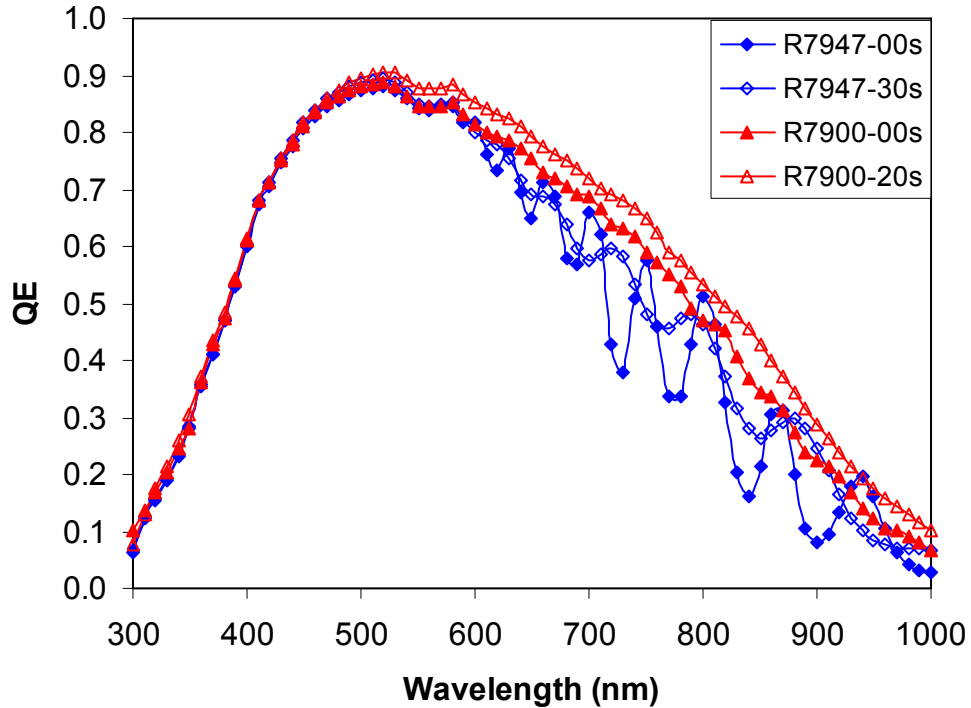


Figure 6. QE curves for nc-Si:H solar cells deposited on different BRs as described in Table II.

intrinsic layer in the nc-Si:H cells is over 1 μm thick, which is a few times larger than the relevant wavelength of the light in the spectrum (taking the wavelength compression factor into account). Certain light scattered at small angles θ may reach the condition of total internal reflection at the semiconductor/ITO interface or the ITO/air interface, and hence the light can be trapped in the semiconductor layers with multiple passes. In addition, the growth of nc-Si:H also produces extra features as previously observed. Therefore, the growth of nc-Si:H is not conformal with the substrate morphology, and therefore, the effective light trapping can be achieved by large micro-features on the substrate.

1.4 SUMMARY

We have studied the correlations between the preparation conditions and micro-features on the Ag/ZnO BRs as well as solar cell performance. We can control the micro-feature size by adjusting the deposition condition and subsequent chemical etching process. The RMS measured by AFM varies from 30 to 120 nm. For a-SiGe:H, we find that the improved Ag/ZnO BR with large micro-features leads to an enhanced V_{oc} . We believe that the increase in the micro-feature size reduces the density of the sharp peaks on the BR surface and consequently reduces the back diffusion of photo-generated carriers at the n/i and i/p interfaces. It can also decrease the shunt current density. Hence, the cell performance was improved. For nc-Si:H solar cells, a clear gain in the J_{sc} has been observed by increasing the micro-feature size on the BR surface, which is due to the effective light trapping by optimizing surface morphology on the BR.

2. nc-Si:H single junction solar cells made by MVHF method at high deposition rates

2.1. INTRODUCTION

In order to realize the use of nc-Si:H material in solar cell production, a challenge is to reduce the deposition time while remaining good material quality. As mentioned in the last quarterly report, we have explored a new deposition regime to enhance deposition rate in the MVHF technique. Compared to the previous deposition time of 50 minutes for the intrinsic layer, the current intrinsic layer deposition time has been reduced to 20-30 minutes corresponding to a deposition rate of 6-10 Å/s. To accomplish this, a strategy we adopt is to make material under the conditions of high pressure and high VHF power. The use of high pressure is for alleviating the ion bombardment on the film surface caused by the high power. However, a high pressure normally gives rise to serious problems in the uniformity and powder formation. To solve this problem, we have modified the hardware design in the MVHF chamber, which includes reducing the spacing between cathode and anode and changing the gas inlet. As reported in the literature, a small spacing can significantly reduce the powder formation. A new gas inlet is designed to improve the uniformity of the nc-Si:H film. In addition, we have also used the hydrogen dilution profiling technique, which has been proved to be a useful method to control the nanocrystalline evolution and improve the nc-Si:H cell performance. After optimizing the deposition parameters with the new chamber design, we have achieved initial active-area efficiencies of 8.23% and 12.1% with a nc-Si:H single-junction and an a-Si:H/nc-Si:H double-junction structures, respectively, for an active area of 0.25 cm².

2.2. nc-Si:H SINGLE-JUNCTION AND a-Si:H/nc-Si:H DOUBLE-JUNCTION SOLAR CELLS

A proper hydrogen dilution is critical for making high efficiency nc-Si:H solar cells. A low hydrogen dilution ratio normally produces amorphous material, however, a very high hydrogen dilution leads to high crystalline volume fraction and large grain size with high micro void/crack density [7]. The best nc-Si:H solar cells are made under the condition close to the nanocrystalline/amorphous transition. In addition, the nanocrystalline/amorphous transition depends on the chamber structure and other deposition parameters. Therefore, we first optimized the hydrogen dilution ratio using the newly modified chamber. To control the nc-Si:H microstructure evolution, we used hydrogen dilution profiling technique. We kept the ramping profile of the active gas the same for one series of depositions and searched for the optimized hydrogen flow rate. Table III lists several nc-Si:H solar cells with the continually decreased hydrogen flow rates from the first to last row in the intrinsic layer deposition. One can see that both the V_{oc} and the thickness are increased monotonically as the hydrogen flow rates are decreased. When the V_{oc} increases to 0.483 V, as shown in sample RF13300, the J-V curve of the cell already shows mixed phase characteristics as indicated by a low FF and J_{sc} . It seems that it is hard to obtain a V_{oc} larger than 0.5 V at the given substrate temperature. FF shows a very complicated relationship with the hydrogen flow rate. This is because FF is not only determined by the material quality, but it is also very sensitive to the ITO properties and the film thickness. The J_{sc} from the QE measurement first shows an increase, then a drop with decreasing hydrogen flow rate, indicating a reduction of crystalline volume fraction.

Table III: J-V characteristics of a series of nc-Si:H single-junction cells made by MVHF at high deposition rates with various hydrogen flow rates, but all other growth parameters remained the same. The intrinsic layer deposition time was 30 minutes. Three values of FF measured under AM1.5, low intensity blue, and low intensity red lights to calculate the efficiency, and probe the *p/i* interface as well as the bulk properties. *d* represents the thickness of the nc-Si:H layer.

Sample No.	H ₂ (sccm)	V _{oc} (V)	FF			J _{sc} (mA/cm ²)	Eff (%)	d (nm)
			AM1.5	Blue	Red			
13287	1100	0.437	0.505	0.571	0.573	23.70	5.23	940
13288	1000	0.435	0.618	0.583	0.589	22.42	6.03	1000
13289	900	0.452	0.549	0.599	0.604	24.27	6.02	1050
13293	800	0.455	0.632	0.612	0.624	22.77	6.55	1100
13294	700	0.460	0.612	0.605	0.636	22.72	6.40	1170
13299	600	0.470	0.634	0.616	0.656	22.27	6.63	1290
13300	500	0.483	0.551	0.603	0.649	20.99	5.58	1400

It is reported that the substrate temperature has a significant effect on grain size, crystal preferential orientation, hydrogen content, and oxygen-related impurity passivation [8,9]. Therefore, optimizing the substrate temperature is of utmost importance in obtaining a high performance solar cell. Table II lists a series of nc-Si:H solar cells made at different temperatures. The substrate temperature of the intrinsic layer deposition was decreased from the first row (Sample 13294) to last row (Sample 13310). The hydrogen dilution ratio and profiling for all the cells was the same. One can see that the V_{oc} increases from 0.460 V to 0.564 V as the substrate temperature was decreased. In the meantime, the efficiency increases from 6.40% to 8.23%, a new record efficiency for the nc-Si:H single-junction cell made by MVHF at a high deposition rate. Figure 6 shows the J-V characteristics and quantum efficiency of the new champion cell.

Having optimized the growth recipe in single-junction cells, we started to fabricate a-Si:H/nc-Si:H double-junction cells, where the a-Si:H top cell was also made at high deposition rate under high pressure. The intrinsic layer deposition time for the top cell was 8-10 minutes. The highest initial efficiency we obtained so far under this deposition regime is 12.1 %. Figure 2 shows the J-V characteristics and quantum efficiency of the a-Si:H/nc-Si:H double-junction cell with bottom cell deposition time of 30 minutes.

Table IV: nc-Si:H single-junction cells made by MVHF at high deposition rates. The intrinsic layer deposition time was 30 minutes. The substrate temperature in the intrinsic layer deposition was decreased continually from the first to last rows. The other growth parameters remained the same. *d* represents the nc-Si:H thickness.

Sample No.	V _{oc} (V)	FF			J _{sc} (mA/cm ²)	Eff (%)	d (nm)
		AM1.5	Blue	Red			
13294	0.460	0.612	0.605	0.636	22.72	6.40	1170
13324	0.490	0.577	0.648	0.651	24.12	6.82	1200
13348	0.546	0.655	0.671	0.680	22.72	8.13	1180
13310	0.564	0.632	0.670	0.682	23.08	8.23	1270

2.3 SUMMARY

In summary, we have explored a new deposition regime to enhance deposition rate of nc-Si:H solar cells using MVHF method. Compared to the previous deposition, the rate was doubled, and the deposition time was reduced to equal to or less than 30 minutes. A record cell efficiency of 8.23% has been achieved in a single-junction nc-Si:H solar cell. By combining this cell with a top cell also made at high rates, we obtained an initial cell efficiency of 12.14% in an a-Si:H/nc-Si:H double-junction structure.

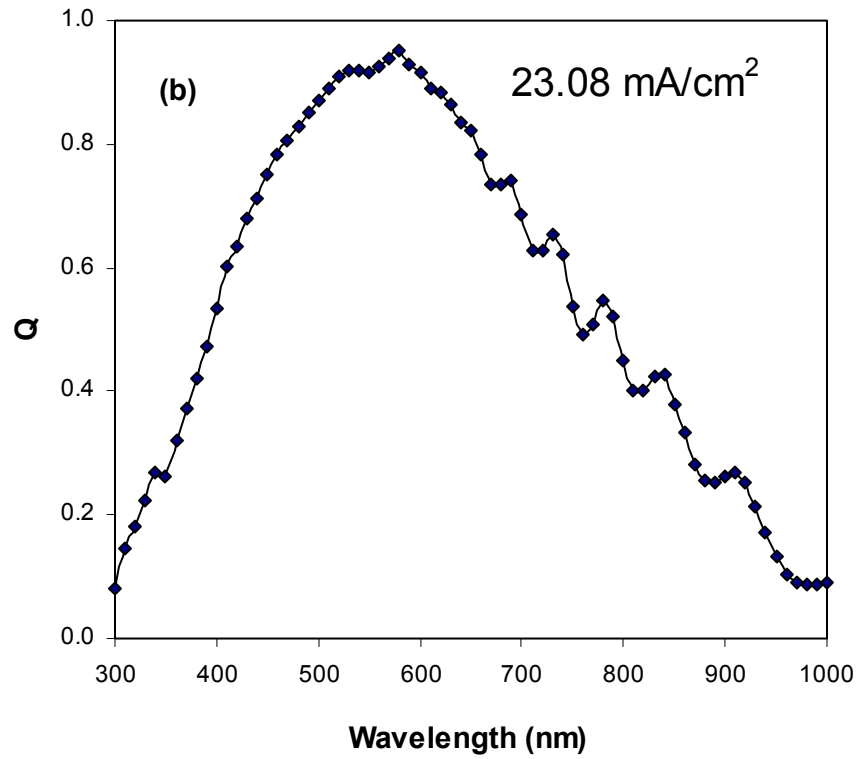
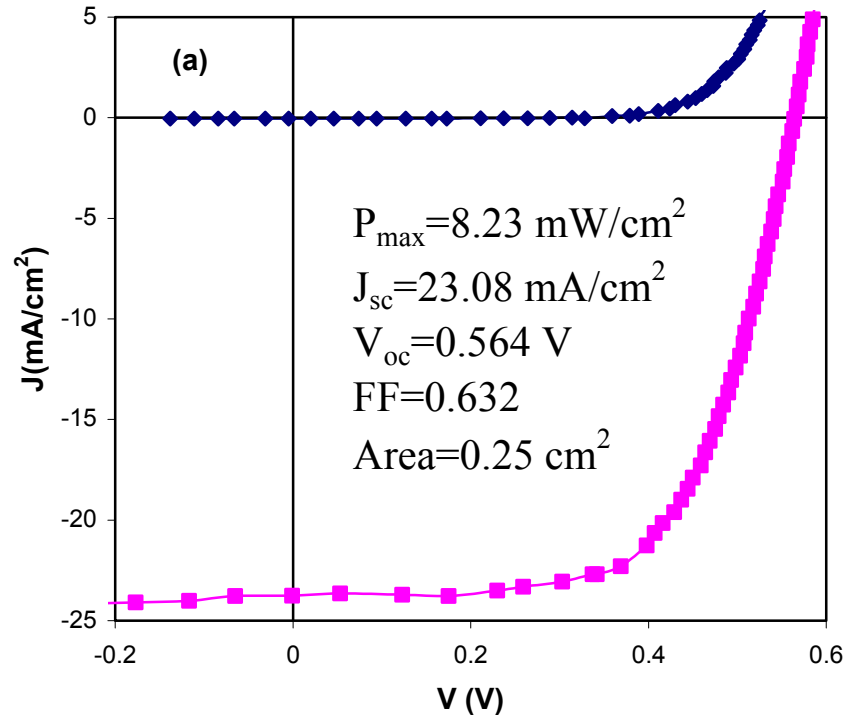


Figure 6. (a) J-V characteristics and (b) quantum efficiency of the nc-Si:H single junction solar cells with the record efficiency of 8.23%.

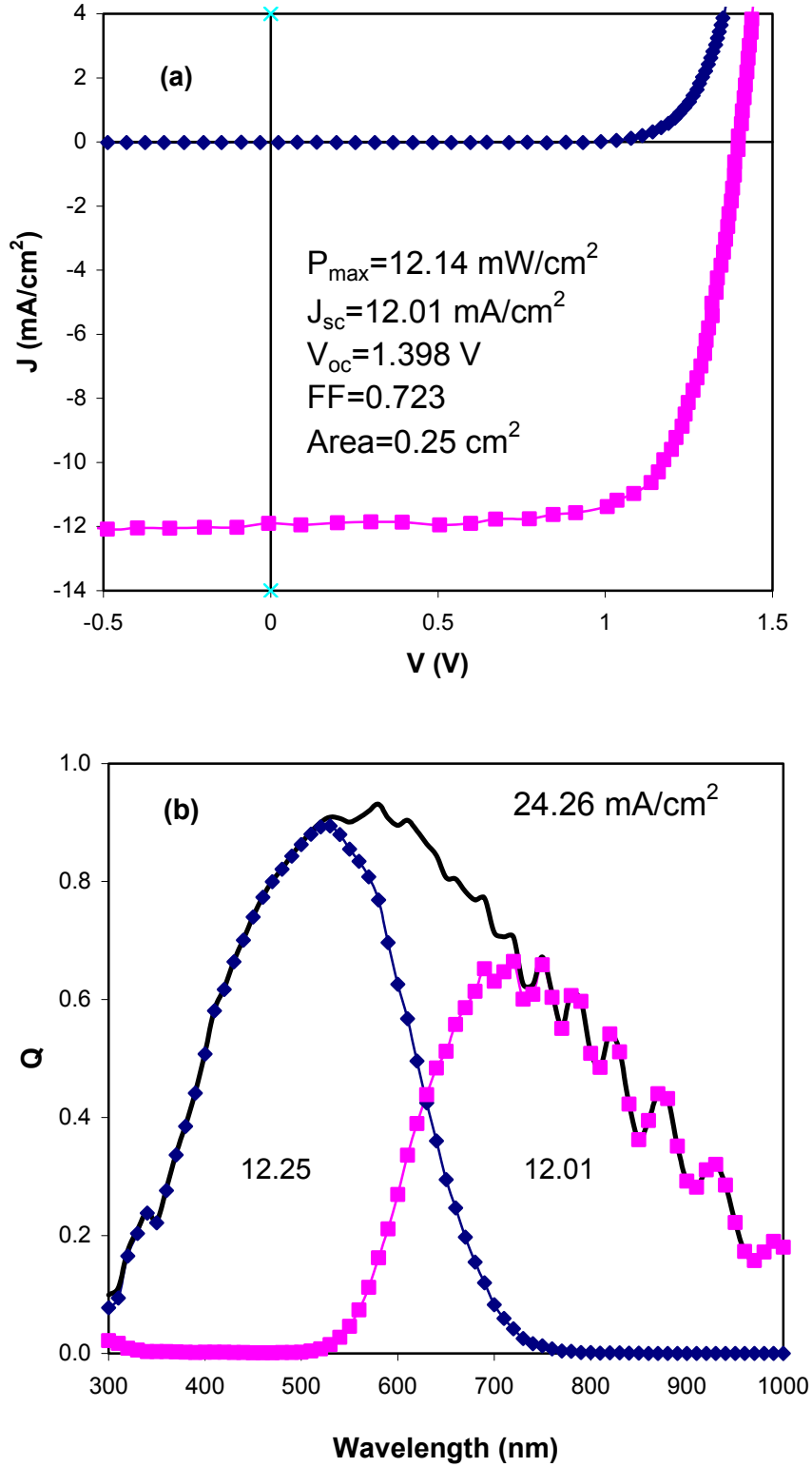


Figure 7. (a) J-V characteristics and (b) quantum efficiency of an a-Si:H/nc-Si:H tandem solar cell, where the deposition times of the intrinsic layers in the bottom and top cells are 30 minutes and 10 minutes, respectively.

3. Large-area deposition of nc-Si:H solar cells at high deposition rate

In our previous quarterly report, we reported an efficiency of 11.6% for an a-Si:H/nc-Si:H tandem cell with the nc-Si:H intrinsic layer deposited in 50 minutes using a combination of a smaller electrode spacing and higher deposition pressure in the large-area machine (2B). We have further optimized the deposition conditions and have now been able to obtain an initial active-area efficiency of 12.0% for a 0.25 cm² cell. The J-V characteristics and QE curves of this cell are shown in Fig. 8. We are now making modules using these optimized conditions.

In our last report we also reported the initial performance of a-Si:H/nc-Si:H double-junction cells using a 3.3Å/s nc-Si:H bottom cell on Ag/ZnO back reflectors (BR) with an aperture area of 45 cm². These cells were light soaked and Table V shows that the degradation is about 9-10% and the stabilized efficiency is ~10.2%. The consistency of the performance over various parts of a larger area is encouraging and we are currently in the process of using these optimized conditions to fabricate a-Si:H/nc-Si:H double-junction modules with 10 times larger areas.

Table V: Initial and light soaked performance of 45.5 cm² a-Si/nc-Si tandem cells.

Serial #	State	Temp (°C)	V _{oc} (V)	I _{sc} (A)	FF	P _{max} (W)	Eff (%)	Eff(%) @ 25°C
10389G2	Initial	21.7	1.425	0.492	0.729	0.512	11.245	11.165
	392h	24.4	1.38	0.499	0.696	0.479	10.53	10.52
	1103h	23.9	1.378	0.491	0.684	0.463	10.17	10.15
	% Degr.		3.32	0.22	6.15	9.62		9.13
10390E2	Initial	21.2	1.415	0.483	0.752	0.514	11.293	11.205
	392h	24.4	1.37	0.512	0.687	0.483	10.61	10.59
	1103h	23.9	1.369	0.488	0.690	0.461	10.13	10.11
	% Degr.		3.28	-1.08	8.27	10.32		9.81
10390F1	Initial	21.2	1.424	0.502	0.72	0.514	11.296	11.208
	392h	24.4	1.38	0.508	0.683	0.477	10.47	10.46
	1103h	23.9	1.377	0.500	0.676	0.466	10.24	10.21
	% Degr.		3.33	0.36	6.04	9.37		8.88
10390F2	Initial	21.5	1.42	0.499	0.732	0.519	11.399	11.315
	392h	24.4	1.37	0.4985	0.688	0.469	10.315	10.305
	1103h	23.9	1.374	0.503	0.673	0.465	10.23	10.20
	% Degr.		3.27	-0.83	8.01	10.33		9.84
10390G1	Initial	21.2	1.424	0.498	0.721	0.512	11.252	11.162
	392h	24.4	1.37	0.518	0.642	0.456	10.02	10.01
	1103h	23.9	1.380	0.504	0.660	0.459	10.08	10.06
	% Degr.		3.08	-1.13	8.44	10.39		9.89

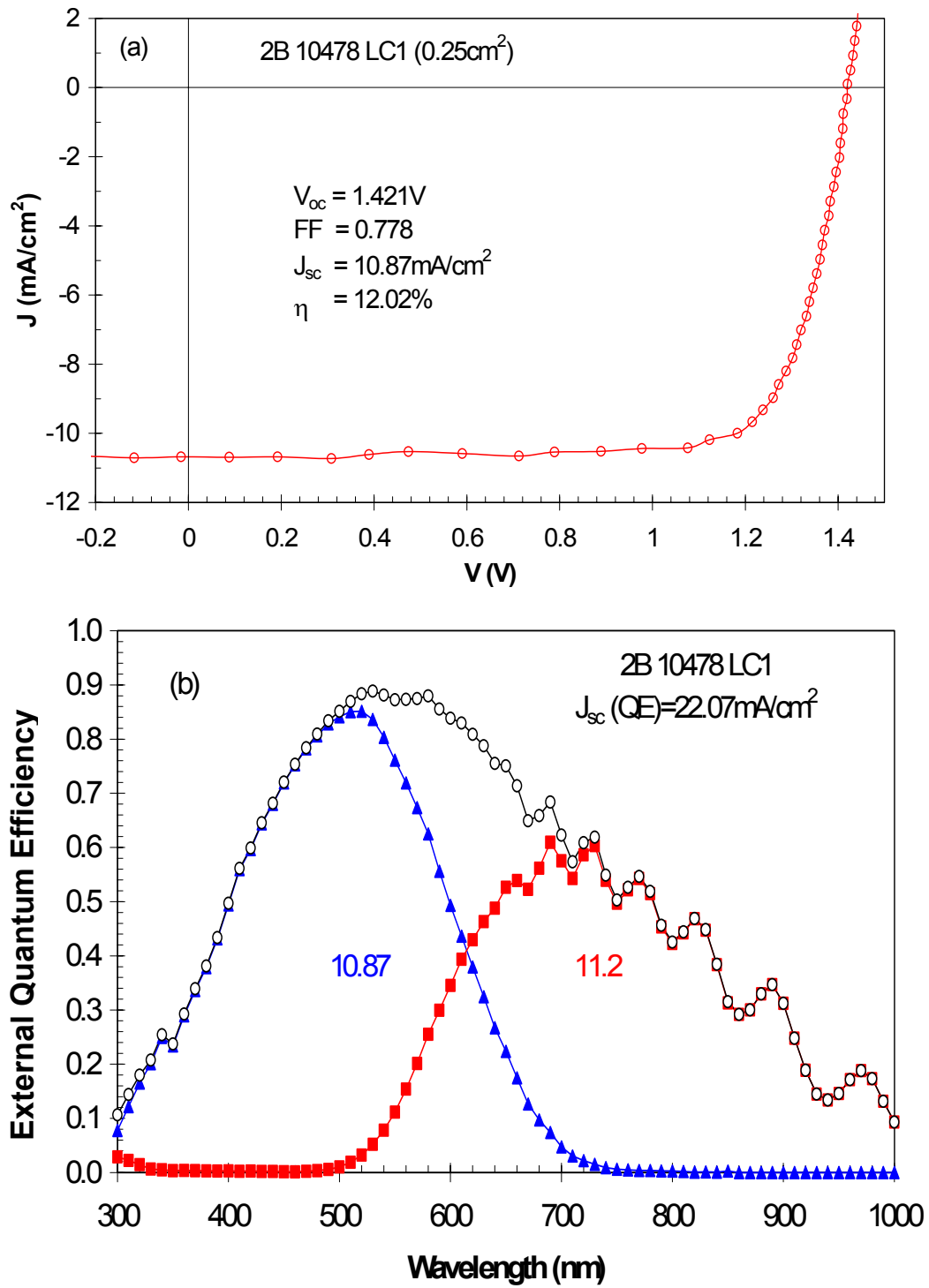


Figure 8. (a) J-V characteristics and (b) quantum efficiency of an a-Si:H/nc-Si:H double-junction solar cell with an active-area (0.25 cm²) efficiency of 12.0%.

4. References

- [1] A. Banerjee and S. Guha, *J. Appl. Phys.* **69**, 1030 (1991).
- [2] J. Yang, A. Banerjee, and S. Guha, *Appl. Phys. Lett.* **70**, 2975 (1997).
- [3] A. V. Shah, J. Meier, E. Vallat-Sauvain, N. Wyrsh, U. Kroll, C. Droz, and U. Graf, *Solar Energy Materials & Solar Cells* **78**, 469 (2003).
- [4] B. Yan, G. Yue, J. Yang, A. Banerjee, and S. Guha, *Mater. Res. Soc. Symp. Proc.* **762**, 309 (2003).
- [5] B. Yan, G. Yue, K. Lord, A. Banerjee, and S. Guha, *Proc. of 3rd World Conf. on Photovoltaic Energy Conversion* (Osaka, Japan, 2003), p. 2773.
- [6] J. Müller, G. Schöpe, O. Kluth, M. Ruske, J. Trube, B. Szyszka, Th. Höing, X. Jiang, and G. Bräuer, *Proc. of 28th IEEE Photovoltaic Specialist Conf.* (Anchorage, AK, 2000), p. 758.
- [7] F. Finger, S. Klein, T. Dylla, A. L. Baia Neto, O. Vetterl, and R. Carius, *Mater. Res. Soc. Symp. Proc.* **715**, 123 (2002).
- [8] Y. Nasuno, M. Kondo, and A. Matsuda, *Appl. Phys. Lett.* **78**, 2330 (2001).
- [9] Y. Nasuno, M. Kondo, and A. Matsuda, *Proc. of 28th IEEE Photovoltaic Specialists Conf.* (Alaska, 2000), p. 142.